JGR Atmospheres

RESEARCH ARTICLE
10.1029/2018JD028825

Acyl Peroxy Nitrates Link Oil and Natural Gas Emissions to High Ozone Abundances in the Colorado Front Range During Summer 2015

Jakob Lindaas[1], Delphine K. Farmer[2], Ilana B. Pollack[1], Andrew Abeleira[2], Frank Flocke[3], and Emily V. Fischer[1]

[1]Department of Atmospheric Science, Colorado State University, Fort Collins, CO, USA, [2]Department of Chemistry, Colorado State University, Fort Collins, CO, USA, [3]National Center for Atmospheric Research, Boulder, CO, USA

Key Points:
- Anthropogenic VOC precursors dominate APN production when ozone is most elevated in the Colorado Front Range in summer 2015
- Propane and n-pentane, primarily from oil and natural gas emissions, drive elevated PPN/PAN ratios during high-ozone events
- Emissions from the oil and natural gas sector contribute to O_3 production on high O_3 days

Supporting Information:
- Supporting Information S1

Correspondence to:
J. Lindaas and E. V. Fischer,
jlindaas@rams.colostate.edu;
evf@rams.colostate.edu

Citation:
Lindaas, J., Farmer, D. K., Pollack, I. B., Abeleira, A., Flocke, F., & Fischer, E. V. (2019). Acyl peroxy nitrates link oil and natural gas emissions to high ozone abundances in the Colorado Front Range during summer 2015. *Journal of Geophysical Research: Atmospheres*, *124*, 2336–2350. https://doi.org/10.1029/2018JD028825

Received 13 APR 2018
Accepted 29 DEC 2018
Accepted article online 3 FEB 2019
Published online 23 FEB 2019

Author Contributions:
Conceptualization: Jakob Lindaas, Delphine K. Farmer, Frank Flocke, Emily V. Fischer
Data curation: Ilana B. Pollack, Andrew Abeleira, Emily V. Fischer
Formal analysis: Jakob Lindaas
Funding acquisition: Delphine K. Farmer, Emily V. Fischer
Methodology: Jakob Lindaas, Emily V. Fischer
Resources: Ilana B. Pollack, Andrew Abeleira, Frank Flocke, Emily V. Fischer
Supervision: Delphine K. Farmer, Emily V. Fischer
Visualization: Jakob Lindaas
Writing - original draft: Jakob Lindaas
(continued)

Abstract We present measurements of ozone (O_3), acyl peroxy nitrates (APNs), and a suite of O_3 precursors made at the Boulder Atmospheric Observatory in Erie, Colorado, during summer 2015. We employ an empirical analysis of the APNs and a previously described positive matrix factorization of the volatile organic compounds (VOCs) to investigate the contribution of different VOC sources to high O_3 abundances at Boulder Atmospheric Observatory. Based on the ratio of peroxypropionyl nitrate (PPN) to peroxyacetyl nitrate (PAN), we find that anthropogenic VOC precursors dominate APN production when O_3 is most elevated. Propane and larger alkanes, primarily from oil and natural gas emissions in the Colorado Front Range, drive these elevated PPN to PAN ratios during high O_3 events. The percentage of OH reactivity associated with oil and gas emissions is also positively correlated with O_3 and PPN/PAN. Idealized box model simulations are used to probe the chemical mechanisms potentially responsible for these observations. We find that observed abundances of long-lived oil and natural gas-related VOCs are likely high enough such that the oxidation of these VOCs in a single photochemical day produces sufficient peroxy radicals to contribute to O_3 formation in the northern Colorado Front Range. Based on our empirical observations and box model simulations, we conclude that oil and natural gas emissions contribute to O_3 production on high O_3 days in this region during summer 2015.

1. Introduction

Formed by the oxidation of volatile organic compounds (VOCs) in the presence of nitrogen oxides (NO_x) and sunlight (Haagen-Smit & Fox, 1956; Sillman, 1999), tropospheric ozone (O_3) negatively affects human health (e.g., Bates, 2005; Ito et al., 2005; Young et al., 1964), especially in sensitive populations such as children and the elderly, and has adverse effects on vegetation (Fowler, 1992). As such, ground-level O_3 is regulated by the U.S. Environmental Protection Agency (EPA) as one of six key criteria pollutants, with the National Ambient Air Quality Standard recently revised to a 70 ppbv maximum 8-hr average (EPA, 2015).

The northern Colorado Front Range metropolitan area (NFRMA) has been in violation of the EPA National Ambient Air Quality Standard for O_3 since 2008 (CDPHE, 2009). Rapid population growth and increasing oil and natural gas development since the early 2000s have changed the quantity and distribution of emissions of many important O_3 precursors (e.g., Evans & Helmig, 2017; McDuffie et al., 2016). However, these emission sources are heterogeneously distributed across the NFRMA (Pfister, Reddy, et al., 2017). NO_x (=NO + NO_2) is emitted predominately from traffic and power generation, and in the NFRMA NO_x is most abundant near major roadways and population centers (Wild et al., 2017; yellow lines and gray areas in Figure 1). These urban areas are also sources of aromatic hydrocarbons, hydrocarbons associated with traffic (e.g., ethyne), and industrial solvents, among other compounds (Swarthout et al., 2013). Oil and natural gas extraction operations in the Denver-Julesberg Basin are clustered in Weld Country around Greeley, Colorado, and extend into areas to the south and west that abut the northern Denver metropolitan area (blue dots in Figure 1). Oil and natural gas activities emit a range of alkanes and aromatic hydrocarbons (Gilman et al., 2013; Halliday et al., 2016; Pétron et al., 2012; Pétron et al., 2014; Thompson et al., 2014). Biogenic emissions from dispersed broadleaf trees throughout urban neighborhoods in the NFRMA contribute small amounts of isoprene, and needle-leaf forests in the Rocky Mountain foothills along the western edge of the NFRMA have been shown to emit small amounts of several alkene species (Rhew et al., 2017).

Writing – review & editing: Jakob Lindaas, Delphine K. Farmer, Ilana B. Pollack, Andrew Abeleira, Frank Flocke, Emily V. Fischer

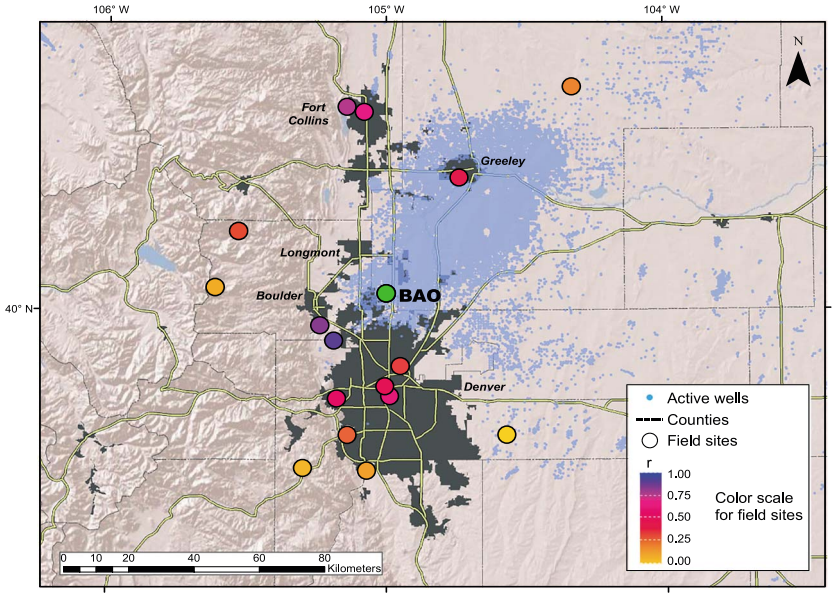

Figure 1. Positive correlations of maximum daily O_3 at Boulder Atmospheric Observatory (BAO) with air quality monitoring sites in the Northern Colorado Front Range for the study period 11 July to 15 August 2015. Dark gray regions are urban areas, with yellow lines representing major roads and dotted lines delineating county boundaries. Small blue dots are the locations of active oil and natural gas wells. Large points are 14 CDPHE air quality monitoring sites, as well as the CASTNET Rocky Mountain National Park site and the NOAA Niwot Ridge location. These are sites that measure O_3 and are colored by the correlation coefficient between daily maximum hour-averaged O_3 mixing ratios the measured that location and BAO. For sites that routinely exceed the National Ambient Air Quality Standard (https://www.colorado.gov/airquality/html_resources/ozone_summary_table.pdf; Rocky Flats N, NREL, Fort Collins West, Welch, Chatfield State Park, and Greeley Weld Tower), correlation coefficients with BAO are $r = 0.77$, 0.67, 0.76, 0.54, 0.47, and 0.57, respectively.

Photolysis of NO_2 is the only known mechanism for chemically producing O_3 in the troposphere (Monks et al., 2015). Net O_3 production occurs when NO is recycled back to NO_2 without the subsequent destruction of O_3. Oxidation of VOCs offers a way to convert NO to NO_2 while cycling HO_x, thereby propagating or catalyzing the formation of O_3. This formation of O_3 is initiated by the reaction of OH with a VOC, which begins a process whereby NO_x is interconverted as the VOC oxidation products are further oxidized.

The hydroxyl radical (OH) is the primary daytime oxidant for most VOC species. The VOC OH reactivity (OHR) is then defined as the product of the rate constant associated with the reaction of a species with OH ($k_{OH,\ VOC}$) and the concentration of that species. OHR provides information on which species are likely to initiate the catalytic O_3 production cycle. OHR does not, however, give insight into how oxidation products of that VOC may propagate or terminate the NO_x and HO_x catalytic cycles.

The oxidation pathways of most VOCs are complex, and the fate of oxidation products (such as RO and RO_2 radicals) plays a large role in the extent to which the reactions supporting catalytic O_3 production continue or whether these cycles terminate. This leads to complex and nonlinear chemistry that is impacted by the relative abundances of NO_x and VOCs. Reactions that terminate the cycling of NO_x and HO_x can be temporary or permanent sinks for these radical families and include the production of nitric acid, hydrogen peroxide, organic nitrates, and acyl peroxy nitrates (APNs; e.g., Farmer et al., 2011; Sillman et al., 1995; Thornton et al., 2002).

Acyl peroxy nitrates are secondary species that are formed concurrently with O_3 from specific VOC precursors. Therefore, the relative abundances of different APN species offer important evidence for the extent to which their respective parent VOCs impacted the photochemistry of a given air mass. The most common APN, peroxyacetyl nitrate (PAN), also has the widest variety of VOC precursors (Fischer et al., 2014). Comparatively, two other commonly measured APNs, peroxypropionyl nitrate (PPN) and peroxymethacryloyl nitrate (MPAN), have more limited VOC precursors. PPN is formed from oxidation products of primarily anthropogenic VOCs (Roberts et al., 2001), and the main precursor of MPAN is isoprene, a primarily

biogenic species (Williams et al., 1997). APNs are only a temporary sink for NO_x, due to thermal dissociation. The effective thermal lifetime depends on the ratio of NO_2 to NO in a given environment. APNs are also lost via dry deposition, photolysis, and reaction with OH; the rate constants for the reaction with OH differ substantially for individual APNs. Deposition in the nighttime boundary layer likely contributes to the low observed APN abundances overnight at Boulder Atmospheric Observatory (BAO). Thus, most of the variability in day-to-day daytime measured APN mixing ratios in the Front Range is due to local photochemical production or to the movement of different Front Range air masses toward BAO. One notable exception is the presence of wildfire smoke, which can contain substantial amounts of PAN (e.g., Lindaas et al., 2017).

In this study we explore the contribution of different VOC precursors to high O_3 events at the BAO in summer 2015. We build upon previous measurements made at BAO during summer 2014 and report similar patterns in the relationships between measured APN species and O_3. We pair this analysis with a concurrently measured data set of 40+ VOCs (Abeleira et al., 2017) and examine the empirical relationships between different VOC sources, O_3, and APNs. Next, we present several idealized box model simulations to probe the underlying mechanisms for the empirical relationships we observe. Lastly, we use the box model to investigate the primary precursors of PPN and provide support for the hypothesis presented in Zaragoza et al. (2017) that alkane precursors dominate the production of APNs in the NFRMA.

2. Data and Methods

2.1. Research Location and Data

During summer 2015 (1 July to 7 September 2015), a suite of trace gasses were measured at the BAO, located north of Denver, Colorado, in the middle of the northern Colorado Front Range (40.05°N, 105.01°W, 1584 m above sea level). Decommissioned in 2016, BAO had a long history of atmospheric trace gas and meteorological measurements (Gilman et al., 2013; Kelly et al., 1979). The suite of O_3 precursor species and photochemical products measured in summer 2015 included nitrogen oxides (NO and NO_2), total reactive nitrogen (NO_y), a set of 45 organic compounds (including selected alkanes, alkenes, C –C_2 halocarbons, alkyl nitrates, and several oxygenated VOCs), three APN species (PAN, PPN, and MPAN), CO, and CH_4. These measurements were made by instruments housed in two trailers located at the base of the BAO tower with inlet heights of 6 m above ground level [agl]; all data are available at the National Oceanic and Atmospheric Administration (NOAA) website (https://esrl.noaa.gov/csd/groups/csd7/measurements/2015songnex/). Full details of the measurement techniques and instrument descriptions have been previously published in Abeleira et al. (2017) and Lindaas et al. (2017). O_3 data used in this analysis were collected by the NOAA Global Monitoring Division surface ozone network (data available at aftp.cmdl.noaa.gov/data/ozwv/SurfaceOzone/BAO/). The inlet location was about 50 feet from the two trailers at 6 m agl on the BAO tower. A full description of the measurement technique used in the collection of these data is presented in McClure-Begley et al. (2014).

This analysis uses measurements from the period 11 July to 15 August 15. The days within the campaign study period but before and after 11 July to 15 August have been determined to be impacted by aged wildfire smoke (Lindaas et al., 2017). Data used in this analysis are further restricted in two ways. Analysis using the APN measurements is restricted to 18 July to 15 August because prior to this date the MPAN peak was compromised. Valid VOC measurements for this analysis were likewise restricted to 24 July to 14 August due to water issues in the gas chromatograph system (Abeleira et al., 2017).

2.2. PMF Factors

Abeleira et al. (2017) characterized the VOC measurements made at BAO during summer 2015. They used positive matrix factorization (PMF) to differentiate multiple source classifications and to partition the species measured among these factors. For summer 2015 they identified six source factors: short-lived oil and gas, long-lived oil and gas, traffic, secondary, biogenic, and background.

Here we use the reconstructed time series of the summed OH reactivity (OHR) for these factors to investigate the empirical connections between these source classifications and our secondary species of interest, O_3, and the APNs. The reconstructed OHR time series was created by calculating the OHR of each species, using the time series of the reconstructed mixing ratios for that species, the temperature-dependent $k_{OH,\ VOC}$, and the

ambient 10-m air temperature time series, and then aggregating the reconstructed OHR time series across all species in a given factor. For simplicity, we group the short- and long-lived oil and gas factors into one oil and gas factor and note that the biogenic factor solely consists of isoprene.

2.3. Box Model Setup

We use BOXMOX (Knote et al., 2015; https://boxmodeling.meteo.physik.uni-muenchen.de/online_tools/boxmox.html), an online extension to the Kinetic PreProcessor (Sandu et al., 2003), to investigate mechanisms that may be responsible for our empirical observations. We use the full set of equations from the Master Chemical Mechanism (MCM) version 3.3 (Emmerson & Evans, 2009; Jenkin et al., 2015) with fixed environmental parameters in a zero-dimensional framework to simulate idealized photochemistry in the Front Range, summarized in Table 1. The MCM explicitly simulates thousands of reactions and has been extensively used in past studies of urban photochemistry (e.g., Sommariva et al., 2011). For all simulations, we held the mixing height constant at 1 km and the ambient temperature at 300 K. The mixing height value is only used to guide the calculation of the immediate even mixing of chemical emissions. In this way the mixing ratio achieved by addition of emissions can be changed by either adjusting the emissions or the mixing height. Here we keep mixing height constant and adjust emissions to change abundances of relevant species, fully described below. No deposition, turbulent mixing, or entrainment/dilution parameters are included. The simulations are run for 8 hr at a 10-min time step. While we are not attempting to recreate specific high-O_3 events, 8 hr is roughly the length of the photochemically active part of 1 day, and it is long enough for us to test and compare mechanisms behind 1 day of photochemical O_3 production under different mixtures of O_3 precursors. We did test the sensitivity of our inferences to the length of time we ran the model for. The conclusions we draw from our 8-hr simulations are not changed when the model is run for 24 hr. Photolysis rates were calculated from the National Center for Atmospheric Research Tropospheric Ultraviolet and Visible (TUV; Madronich, 1992) radiation model for 40°N and 105°W, 1,700 m agl. The full set of TUV parameters are listed in Table S1 in the supporting information. The photolysis rates were held constant for the duration of each simulation.

Additionally, NO and NO_2 emissions are added at each time step such that NO_x mixing ratios stay approximately constant throughout each simulation. The goal of this setting is to allow VOC oxidation to proceed under an approximately consistent VOC/NO_x regime in each simulation.

BOXMOX simulations are initialized with four different VOC mixtures. The four mixtures include a baseline mixture ("baseline"), a high oil and natural gas influenced mixture ("high ONG"), a high traffic influenced mixture ("high traffic"), and a high biogenic mixture wherein a small quantity of isoprene (3×10^{11} molec·cm^{-2}·s^{-1}) was emitted into the box at every time step to keep isoprene approximately constant throughout the simulation ("isoprene addition"). Initial mixing ratios in the "baseline" are initialized with the median value of every measured VOC for the measurement period between daytime hours of 10 a.m. to 6 p.m. MDT, while the three other mixtures are created by adding the mixing ratio equivalent of 0.5 s^{-1} of OH reactivity, distributed among respective sets of species, to the baseline initial conditions. Thus, the high ONG mixture has an additional 0.5 s^{-1} of OHR, achieved by proportionately increasing the initial mixing ratios of species that were unambiguously factored into the combined oil and gas PMF factor in Abeleira et al. (2017). Accordingly, species that are predominately associated with the traffic PMF factor are proportionately increased by 0.5 s^{-1} OHR mixing ratio equivalent to create the high-traffic mixture. VOCs that were not measured at our research location were initialized in all simulations to 0 ppbv. We recognize that this decision means we are missing potentially important sources of OHR. However, we measured many of the most abundant VOCs (Abeleira et al., 2017), and a full representation of all possible species is not needed for our primary goal: to investigate chemical mechanisms that may underpin our empirical observations. APNs and alkyl nitrates were also not given initial concentrations, meaning the presence of these species in the output of the simulations is solely due to secondary production.

Values for all initial mixing ratios of species present in each mixture are summarized in Table 1. Species that were not unambiguously factored into a single PMF factor are initialized at constant mixing ratios across the simulations. These species are listed at the bottom of Table 1 (mixed source species). This is a limitation to our approach, because we expect there to be influences from certain sectors on their abundances. For example, of the VOCs measured in summer 2015, acetaldehyde is the largest contributor to OHR (17%). Several of

Table 1
Initial Conditions for All BOXMOX Simulations

	Baseline	High ONG	Isoprene addition	High traffic
Temperature		300 K		
Mixing Height		1000 m		
Deposition		NA		
Turbulent Mixing		NA		
Entrainment		NA		
Photolysis Rates		constant, from TUV[a]		
NO emissions[b]		3×10^{11} molec·cm^{-2}·s^{-1}		
NO_2 emissions[b]		3×10^{10} molec·cm^{-2}·s^{-1}		
Isoprene emissions	0	0	3×10^{11} molec·cm^{-2}·s^{-1}	0
NO[b]		0.5 ppbv		
NO_2[b]		1 ppbv		
O_3		50 ppbv		
H_20		1%		
CH_4		1,900 ppbv		
CO		110.9 ppbv		
M		1e9 ppbv		
N_2		78.084%		
O_2		20.946%		
OH		0 ppbv		
Initial $\sum OHR_{voc}$ (s^{-1})	1.58	2.08	2.08	2.08

Oil and natural gas species (ppbv)

	Baseline	High ONG	Isoprene addition	High traffic
Ethane	5.4	12.5	5.4	5.4
Propane	2.39	5.5	2.39	2.39
i-butane	0.41	0.96	0.41	0.41
n-butane	1.0	2.32	1.0	1.0
i-pentane	0.9	2.08	0.9	0.9
n-pentane	0.71	1.64	0.71	0.71
n-hexane	0.1	0.23	0.1	0.1
Cyclohexane	0.053	0.12	0.053	0.053
2-methylhexane	0.024	0.056	0.024	0.024
n-heptane	0.042	0.097	0.042	0.042
n-octane	0.021	0.049	0.021	0.021
cis-2-butene	0.016	0.037	0.016	0.016
Benzene	0.091	0.211	0.091	0.091

Traffic species (ppbv)

	Baseline	High ONG	Isoprene addition	High traffic
Toluene	0.111	0.111	0.111	2.07
Ethylbenzene	0.012	0.012	0.012	0.22
Ortho-xylene	0.015	0.015	0.015	0.28
Ethyne	0.14	0.14	0.14	2.61
3-methylhexane	0.02	0.02	0.02	0.372

Biogenic species (ppbv)

	Baseline	High ONG	Isoprene addition	High traffic
Isoprene	0.167	0.167	0.167	0.167

Mixed source species (ppbv)

	Baseline	High ONG	Isoprene addition	High traffic
Ethene	0.123	0.123	0.123	0.123
Propene	0.035	0.035	0.035	0.035
Acetaldehyde	1.915	1.915	1.915	1.915
Acetone	3.16	3.16	3.16	3.16
MEK	0.344	0.344	0.344	0.344
CH_2Cl_2	0.021	0.021	0.021	0.021
$CHCl_3$	0.007	0.007	0.007	0.007

Note. All environmental parameters and NO_x emissions were held constant throughout the simulations, which were run for 8 hr at 10-min time steps. Initial conditions for the simulations are given for a NO_x scaling factor of 1.
[a]TUV input parameters given in Table S1. [b]Multiply by the NO_x scaling factor if needed.

the alkanes are precursors for acetaldehyde (Millet et al., 2010), but the background and secondary factors in Abeleira et al. (2017) accounted for the majority of this species.

We compared the NO_2/NO ratio in our simulations to that observed at BAO. For all of our simulations, the initial NO_2/NO ratio was ~2, but the NO_2/NO ratio adjusts within 2–3 time steps (10 min each) to a level consistent with the average ratio of the BAO field measurements (~5). OH concentrations in all simulations were also similar to those measured in the NFRMA during the Front Range Air Pollution and Photochemistry Experiment aircraft campaign in summer 2014 (Ebben et al., 2017). Additionally, we tested the sensitivity of each simulation to NO_x by running each VOC mixture with a series of five NO_x scaling factors: 0.25, 0.5, 1, 2, and 3. With all other initial conditions held constant, both the NO and NO_2 initial conditions and NO and NO_2 emissions at each time step are multiplied by the given NO_x scaling factor (i.e., a simulation run with a NO_x scaling factor of 2 contains twice as much NO_x as a simulation run with a scaling factor of 1). At the original level of NO_x (NO_x scaling factor of 1), we find that our simulations are close to peak O_3 production efficiency. For NO_x scaling factors of 0.5 and 2, O_3 production does not change significantly, but for a factor of 3 increase or decrease in NO_x (scaling factors of 3 and 0.25), we find much less efficient O_3 production in all simulations. Abeleira and Farmer (2017) used an empirical analysis to find that O_3 production in the northern Colorado Front Range is likely near peak O_3 production efficiency. Though their analysis was specific to the Denver metro area and spatial heterogeneity likely exists in the O_3 production efficiency across the northern Colorado Front Range, our conclusions are not affected by changing the NO_x scaling factor by a factor of 2. Thus, we use a NO_x scaling factor of 1 in all simulations discussed in this paper.

3. Empirical Results

3.1. Spatial Variability in NRFMA O_3 and Its Precursors

Strong spatial gradients in emissions and meteorology in the NFRMA make this region particularly heterogeneous (Pfister, Reddy, et al., 2017). The sources of O_3 precursors differentially impact ground-level O_3 across the Front Range. Denver and surrounding suburban and industrial areas (large gray area in Figure 1) are characterized by large NO_x emissions and certain VOC emissions. Outside of Denver and its suburbs there are also several more disperse population centers (e.g., the cities of Boulder, Longmont, Fort Collins, and Greeley), and oil and natural gas production closely border, if not overlap these population centers (small blue dots in Figure 1). Though likely less relevant for O_3 production, agricultural activities are also a major source of atmospheric compounds in the Front Range (Eilerman et al., 2016; Tevlin et al., 2017; Townsend-Small et al., 2016). Recirculation and upslope-downslope regimes mix these sources of emissions throughout the NFRMA (Pfister, Reddy, et al., 2017; Sullivan et al., 2016; Vu et al., 2016).

The BAO was located north of the Denver urban area and at the southeast corner of the region with the most dense oil and gas development. This site has hosted a variety of recent field experiments focused on atmospheric chemistry and air quality. For example, in situ observations from this location have been used to investigate specific aspects of nighttime chemistry (Brown et al., 2013), the relative importance of different sources on VOC abundances in the Colorado Front Range (e.g., Abeleira et al., 2017; Gilman et al., 2013; Pétron et al., 2014; Swarthout et al., 2013), and the impact of oil and gas emissions on summertime O_3 chemistry in this region (McDuffie et al., 2016). Recent measurements near BAO in Erie, Colorado, indicate that atmospheric composition near BAO is similar to other sites throughout the northern Colorado Front Range in the types of species present and their relative abundances (Thompson et al., 2014). Analogously, we find that O_3 measurements at BAO are positively correlated with O_3 measurements across the Front Range. Figure 1 shows the correlation coefficient (r) of the relationship between daily maximum hour-averaged O_3 mixing ratios at BAO and daily maximum 1-hr averaged O_3 mixing ratios at 14 CDPHE air quality monitoring sites as well as the CASTNET Rocky Mountain National Park site and the NOAA Niwot Ridge location. Correlation coefficients >0.6 exist for most sites along the Denver to Fort Collins corridor, with lower correlations between BAO and further afield sites such as rural Weld County and east Aurora. Variability of O_3 abundances is also similar at BAO as compared to other sites. Specifically, the standard deviation in maximum hourly O_3 mixing ratios at BAO (10.5 ppbv) is comparable to the median standard deviation (9.9 ppbv) of all locations, and it is also within the range of standard deviations (5.5–12.2 ppbv) at other Front Range locations.

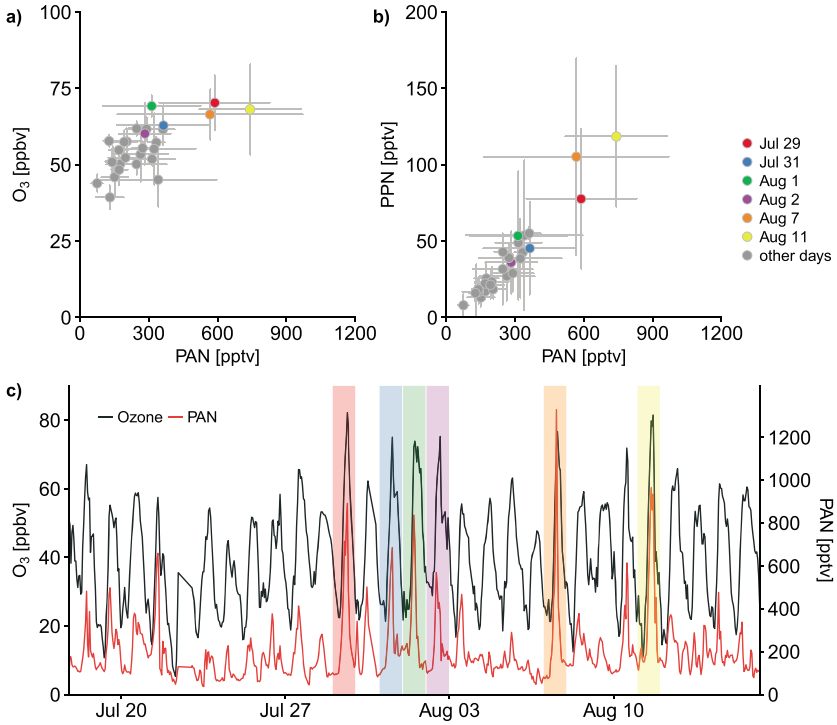

Figure 2. Relationship between (a) O_3 and peroxyacetyl nitrate (PAN) and (b) peroxypropionyl nitrate and PAN. Points represent afternoon (12 p.m. to 6 p.m. MDT) average mixing ratios for each day during the study period. Error bars indicate +/−1 standard deviation. (c) Time series of O_3 in black and PAN in red. The colors of the rectangular shading denote the corresponding days in panels (a) and (b).

3.2. Ozone and APNs

APNs are considered to be excellent tracers of photochemical activity because they are not directly emitted (Fischer et al., 2014). Prior work based on observations from summer 2014 showed that APN species at BAO are good tracers of local photochemistry (Zaragoza et al., 2017). Conversely, periods of elevated O_3 driven by long-range transport or a large contribution of O_3 from the upper troposphere in 2014 were not found to be associated with elevated APNs (Zaragoza et al., 2017). During summer 2015, we do not find any days in our study period that display evidence of long-range transport or stratospheric intrusion. Significant periods during our measurement campaign were influenced by wildfire smoke (Lindaas et al., 2017), including several days with high O_3, but these periods are not included in this analysis.

Similar to prior measurements at BAO and other locations, Figure 2a shows a positive relationship ($R^2 = 0.51$) between afternoon average (12 p.m. to 6 p.m. MDT) O_3 and PAN mixing ratios over the study period. Zaragoza et al. (2017) also found a strong relationship between PPN and PAN, and Figure 2b indicates a similar strong relationship during summer 2015 ($R^2 = 0.93$). The ratio of PPN to PAN can tell us about the precursors that dominated the secondary production preceding a given measurement (Roberts et al., 1998). Zaragoza et al. (2017) hypothesized that PPN/PAN ratios >0.15 were indicative of alkane-dominated photochemistry in the Front Range, and we discuss this further in later sections. Figure 2c presents the time series of hourly average O_3 and PAN mixing ratios for summer 2015. The shaded colors designate 6 days with the highest maximum hourly average O_3 abundances. These same colors are used to denote the corresponding points in panels (2a) and (2b). These 6 days are not only among the days with the highest daily average O_3 but are also associated with hourly PAN mixing ratios >500 pptv. Similar to the observations from summer 2014 (Zaragoza et al., 2017), we again find that MPAN is closely correlated with PAN ($R^2 = 0.69$) and PPN ($R^2 = 0.72$) as well, but the absolute mixing ratios we observe (afternoon mean = 8.3 pptv) are low compared to other regions, such as the southeastern or northeastern United States, which have larger isoprene emissions (e.g., Roberts et al., 1998, 2003, 2007).

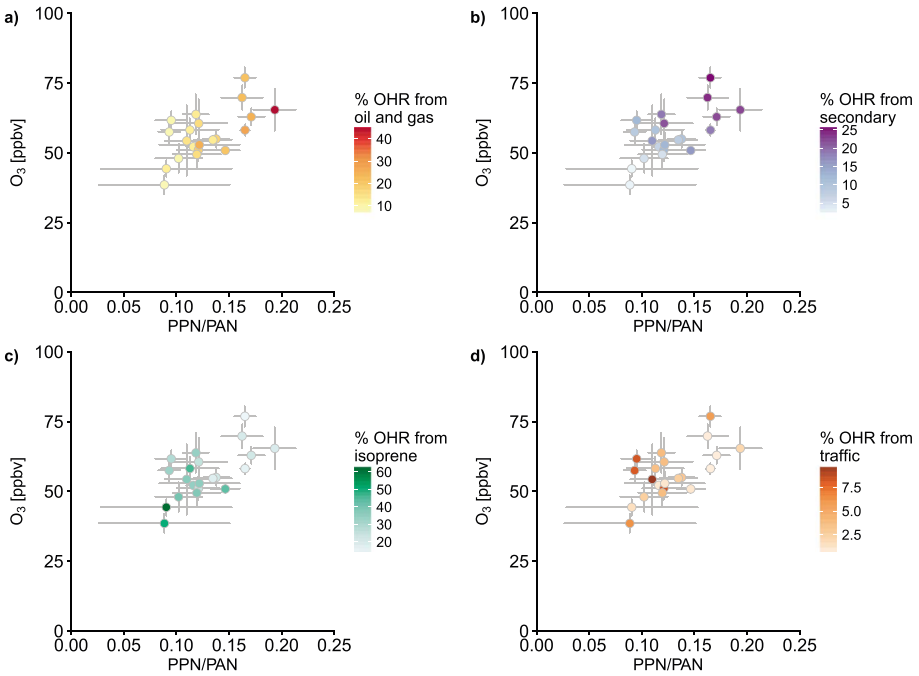

Figure 3. Afternoon (12 p.m. to 6 p.m. MDT) average O_3 mixing ratios versus the ratio of peroxypropionyl nitrate (PPN) to peroxyacetyl nitrate (PAN) at Boulder Atmospheric Observatory for each day during the study period. Error bars indicate +/−1 standard deviation. Points are colored by (a) the percentage of total calculated hydroxyl radical reactivity (OHR) from the oil and natural gas positive matrix factorization (PMF) factor; (b) the percentage of total calculated OHR from the secondary PMF factor; (c) the percentage of total calculated OHR from the biogenic PMF factor, which consists exclusively of isoprene; and (d) the percentage of total calculated OHR from the traffic PMF factor.

3.3. Ozone, PPN/PAN, and VOCs

We observe a positive relationship between afternoon average (12 p.m. to 6 p.m. MDT) O_3 mixing ratios and the ratio of PPN/PAN ($R^2 = 0.41$; Figure 3), suggesting that there is increasing influence from PPN precursors when O_3 abundances are higher in the Front Range. The colors in Figure 3 designate the percentage of total calculated VOC OH reactivity (OHR) from various PMF VOC factors identified by Abeleira et al. (2017); see section 2.3. This percentage is calculated as the sum of OHR for individual species in the factor divided by the summed OHR across all species in all factors. Figure 3a shows that when the PPN/PAN ratio is high, the percentage contribution of oil and gas OHR to total OHR is also high. Conversely, Figure 3c shows that when PPN/PAN is low, the percentage contribution of biogenic species (largely isoprene) to OHR is high. The ratio of MPAN/PAN is also anticorrelated with O_3, following the same pattern as the percentage of biogenic OHR. Other measured secondary species such as alkyl nitrates that are included in the secondary factor are positively correlated with PPN/PAN (Figure 3b). This is to be expected, given this group of secondary species predominately have alkane precursors. Lastly, the percentage of OHR attributed to traffic shows no relationship with PPN/PAN and is consistently below 10% of the total estimated OHR (Figure 3d).

While these observations support the conclusion that oil and natural gas emissions make an important contribution to high O_3 abundances at BAO, it is clear that the variability in PPN/PAN and OHR from the oil and gas factor do not explain all of the variability in O_3 mixing ratios. Meteorological factors such as temperature, relative humidity, and stagnation events have been shown to drive variability on multiple time scales in the NFRMA (Reddy & Pfister, 2016) and other regions (e.g., Camalier et al., 2007; Jacob et al., 1993; Sillman & Samson, 1995). We do not find a relationship between mean afternoon air temperatures or mean afternoon relative humidity measured at BAO and mean afternoon O_3 abundances during our time period. We do, however, find a negative relationship between mean afternoon wind speed and mean afternoon O_3 ($R^2 = 0.52$), such that lower wind speeds are linked to high O_3 and vice versa. These low wind speed days likely exhibit lower ventilation or stagnation. This relationship is strong enough to explain some of the

variability unexplained by PPN/PAN. This is not necessarily inconsistent with our inferences based on atmospheric composition made above; under more calm conditions emissions would have time to build up and react, increasing the potential for oil and gas emissions to contribute to O_3 production. Lower wind speeds are typical of mountain-valley circulation patterns, which often drive local circulation during summer high-pressure events in the NFRMA (Vu et al., 2016).

Another factor that may contribute to variability in measured surface mean afternoon O_3 is the residual O_3 from the previous day. O_3 produced during the previous day persists in the residual layer and can be entrained into the planetary boundary layer the next day as it develops. This residual O_3 will then influence the "starting" mixing ratio as O_3 production begins. There can be considerable variability in this residual O_3 (McDuffie et al., 2016), but without coincident O_3 LIDAR measurements at BAO such as those during summer 2014 (Wang et al., 2017), it is difficult to estimate. We also expect that PAN and PPN will remain aloft in the residual layer and that they are likely also entrained into the planetary boundary layer during the next day. Thus, we acknowledge this as a source of variability, but we lack the tools to effectively separate out the O_3 or PAN production from the current day from the residual O_3 or PAN component. There are other sources that would contribute to variability in either the PAN or O_3 mixing ratios observed at BAO. APN species and O_3 are produced concurrently in the air mass as it is transported to BAO and reflect the chemistry influenced by the same mixtures. However, it is possible that the air masses reaching BAO started with low NO_x abundances and high VOC mixing ratios. This would be likely for air masses that originated in Weld County, outside of the city of Greeley. En route to BAO, there are multiple opportunities for fresh NO_x emission to be injected into traveling air masses. The changing ratios of NO/NO_2 will affect the thermal lifetime of APNs, as discussed in section 1. In short, there is ample heterogeneity in O_3 and APN precursors to contribute to scatter in the APN-O_3 relationship that is observed at BAO.

It is also worth noting several possible complications to using the mean afternoon estimated PMF factor percentage contributions to total OHR (i.e., VOC measurements made at the same time as O_3 and APNs) as the basis for supporting the conclusions reached by the APN and O_3 relationship analysis. While the VOCs measured in the afternoon may represent different mixtures from those that influenced earlier photochemistry. A possible method for addressing this potential issue could be to use VOC measurements from earlier in the day. However, in that case one must assume that the earlier measurements represent the same air mass and the same emission sources as the air mass measured in the afternoon. We know that there is considerable recirculation in the NFRMA and that complex circulation patterns are common (Sullivan et al., 2016; Vu et al., 2016). Thus, this assumption may not be valid. A more conservative assumption is that the coincident afternoon VOC mixture reflects the same mixture that produced O_3 and APNs, though short-lived species may no longer be present. Very short lived VOCs may contribute to the photochemistry of the air masses en route to BAO, but these VOCs may not have been quantified at BAO because they were also consumed en route. For example, isoprene has a lifetime on the order of an hour (for $[OH] = 10^6$ molec/cm^3) and a light and temperature dependent emission rate (Guenther et al., 2006). Isoprene could have been emitted into an air mass en route to BAO but may have been oxidized before the air mass reaches BAO. However, this oxidization of isoprene would likely produce MPAN, and the very low MPAN abundances observed at BAO do not support the hypothesis that isoprene abundances are large in the region.

Our inference that oil and gas emissions significantly influence high O_3 mixing ratios at BAO is consistent with other recent research. McDuffie et al. (2016) combined observations from two summers (2012 and 2014) at BAO and employed the MCM box model to estimate the average contribution of oil and gas emissions to O_3 production in summer 2014. They found that oil and gas emissions are responsible for about 17% of average local O_3 production at BAO. It is important to note that this was an estimate of the average contribution, as McDuffie et al. (2016) did not have temporally collocated measurements available to make specific estimates during high O_3 days in 2014. Evans and Helmig (2017) partitioned O_3 measurements made over 4 years (2009–2012) at two Front Range locations by wind direction and observed that a majority of elevated O_3 measurements were characterized by transport from areas with large oil and gas emissions. Cheadle et al. (2017) used measurements from three individual days in Greeley as case studies to show that a larger abundance of oil- and gas-related species is correlated with higher O_3 mixing ratios. And lastly, regional chemical transport modeling conducted by NCAR as a follow up to the Front Range Air Pollution and Photochemistry Experiment indicates that oil and gas and traffic emissions generally make

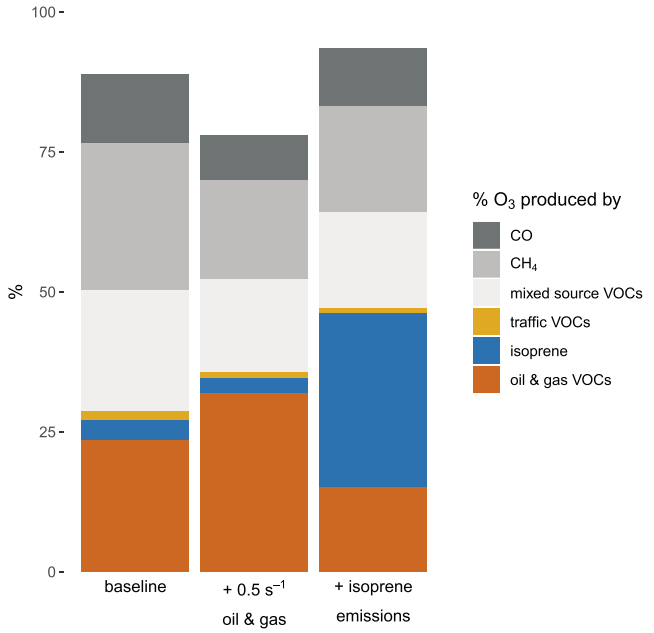

Figure 4. Cumulative percentage contribution to O_3 production by hydrocarbon group for the baseline, high ONG, and isoprene addition simulations, estimated via a local first-order sensitivity analysis over an 8-hr period. VOC = volatile organic compound.

the largest contributions to local O_3 production during summer 2014 in the NFRMA (Pfister, Flocke, et al., 2017).

4. Insights From Idealized Modeling

In this section, we turn to our set of idealized box model simulations to identify possible mechanisms responsible for our empirical results using an explicit chemical framework. For a simulation to be more useful for identifying possible relevant chemical mechanisms than the baseline simulation, it should meet two simple analogy criteria. (1) The initial conditions must be within the measurement ranges for all species, and (2) patterns in the simulated O_3 and APNs must be consistent with the empirical observations. In the empirical analysis outlined in sections 3.2 and 3.3, O_3 and the PPN/PAN ratio are positively related (Figure 3). Of our simulations, only the high ONG simulation meets both of these requirements. After adding 0.5 s^{-1} of OHR equivalent mixing ratios to the ONG species, their total initial mixing ratios still fell within the range of measured abundances. Compared to the baseline simulation, a larger ONG OHR in the high ONG simulation led to increased O_3 production as well as an increase in the PPN/PAN ratio. These outcomes are consistent with the patterns observed in the measurements. Conversely, both the high traffic simulation and the isoprene addition simulation failed at least one of our analogy criteria. With 0.5 s^{-1} of added traffic VOC OHR, the initial mixing ratios of traffic VOCs in the high traffic simulation were nearly an order of magnitude higher than the maximum abundances measured. And though O_3 production was higher than baseline, ratios of PPN/PAN did not increase. Thus, the high traffic simulation is less useful in interpreting the empirical results. As for the isoprene addition simulation, the initial conditions do fall within the bounds of the measurements. However, this simulation produces a lower PPN/PAN ratio compared to the baseline, and a much higher MPAN/PAN ratio. This pattern is inconsistent with the observations, which show that the MPAN/PAN ratio and the amount of isoprene observed at BAO are lower during high O_3 events in summer 2015 compared to low-O_3 periods. This simulation may also be less useful for another reason. Isoprene mixing ratios in the boundary layer are unlikely to be well mixed because it has a shorter chemical lifetime than the likely mixing time for the boundary layer. Initial isoprene abundances and isoprene emissions best reflect surface observations, which are unlikely to represent a boundary layer mean. Thus, based on the application of our two criteria, the high ONG influenced mixture appears to be the most analogous to the observations during high-O_3 events at BAO in summer 2015.

To confirm that the increased O_3 production in the high ONG simulation is driven by the increased abundances of ONG species, we employ a local first-order sensitivity test similar to that performed by Jin et al. (2008) in their investigation of a local high-O_3 episode in the Central Valley of California. In this sensitivity analysis the initial mixing ratios of each group of VOCs as well as CO and CH_4 are perturbed by −10% in separate additional simulations. The difference in the final O_3 abundances between the end of each sensitivity simulation and the original simulation is calculated and multiplied by 10 to approximate the total percentage contribution of that group of VOCs (or CO or CH_4) to the overall O_3 production in the original simulation. This estimate of the total contribution implicitly assumes the impact of each perturbation is linear, and in theory the sum of all percentage contributions will be 1. In practice, given the nonlinearity of O_3 chemistry and the potential for interactions between species, this linearization of the effect is subject to small errors. However, we achieve greater than 80% closure of the overall O_3 production for every simulation. Thus, this local first-order sensitivity analysis is a reasonable approximation of the contribution of each VOC factor to O_3 production in each simulation.

Figure 4 presents the results of this sensitivity analysis for three mixtures: the baseline, the high oil and gas influenced mixture, and the isoprene addition simulation. As expected, the high ONG simulation displays a larger percentage contribution to O_3 production from ONG species (~31% compared to ~23%), and the contribution from isoprene is highest in the isoprene addition simulation. For the reasons outlined above, the

isoprene addition simulation is less representative of the observations and likely contains higher mixing ratios than would exist throughout the full boundary layer. Thus, the contribution from isoprene to O_3 production in the isoprene addition simulation is likely an upper bound, well in excess of the true contribution on high O_3 days. On the other hand, it is possible that the ONG species contribution estimate in the high ONG simulation could actually be a lower bound, given that full closure of O_3 production was not fully achieved by this sensitivity analysis and that the "mixed source VOCs" category includes secondary species such as acetaldehyde and methyl ethyl ketone (MEK) (see Table 1), which have oil- and natural gas-related precursors. For instance, the largest precursor of MEK in the Front Range is likely n-butane, which is largely emitted from oil and natural gas activities. Given that these secondary VOCs have other sources as well, they were not lumped with the group of VOCs we used to represent VOCs largely from oil and gas operations in the region. Traffic VOCs make only a small contribution to O_3 production (< 2%) in all simulations, which is consistent with the empirical observation of low overall percentage contributions of traffic VOCs to measured VOC OHR. CO and CH_4 make significant contributions to O_3 production (8–12% and 17–26%, respectively) in each simulation, which reflects the combination of contributions from background abundances and their local sources in the NFRMA. A large fraction of the locally emitted CH_4 is likely from oil and gas sources, around 75% according to Pétron et al. (2014), but the high hemispheric background of CH_4 means that CH_4 from oil and gas sources contributes a relatively small fraction of the total O_3 production. In our simulations the contribution of the regional oil and gas emissions of CH_4 to total O_3 production is 2%. Overall, the local first-order sensitivity analysis confirms that ONG VOCs are responsible for the increased production of O_3 in the high ONG simulation, which is the most useful simulation for interpreting the observations.

To gain insight into the mechanism behind the increased contribution of ONG VOCs to O_3 production, we tracked the production of peroxy radicals (RO_2) by our different VOC factors. RO_2 species have different parent VOCs, meaning that the relative abundance of certain RO_2 species can offer insight into which parent VOCs are contributing the most to the rate-limiting step in O_3 production. To investigate this, we calculate the relative contribution of different reaction pathways to the formation of NO_2 (and thereby O_3) by tagging RO_2 species according to their precursors and then aggregating the rate at which they produce NO_2 by PMF factor. In this way, we can use RO_2 radicals as a lens into the contribution of different VOCs to O_3 production in our simulations in addition to the first-order sensitivity analysis.

For each VOC associated with a given factor (oil and gas, traffic, or biogenic) we identify every RO_2 produced during the oxidation of that group of VOCs. RO_2 radicals that react with NO to produce NO_2 were then combined into one of five categories: (1) RO_2 radicals that are formed solely from the precursors largely associated with oil and gas activities; (2) RO_2 radicals that are only produced from isoprene oxidation; (3) RO_2 radicals that are only produced from the oxidation of traffic-related precursors; (4) RO_2 radicals with VOC precursors in multiple factors (i.e., they are common products to species in different precursor classes); and (5) the three simplest RO_2 radicals (methyl peroxy, acetyl peroxy, and ethyl peroxy radicals), which are a subset of the common category of RO_2 radicals but were not included in the common category, and often the most abundant RO_2 radicals. We separated out the simplest RO_2 to demonstrate that a large proportion of the RO_2 in all simulations exist as one of these simple C_1–C_2 alkyl peroxy radicals. Thus, we have classified all the RO_2 in the simulations into five categories named "oil and gas RO_2," "biogenic RO_2," "traffic RO_2," "common RO_2," and "simplest RO_2." As an example of a species in the common RO_2 group, both propane and propene are potential precursors for HYPROPO2 ($C_3H_7O_3$) in the MCM, which is a propanol peroxy radical. Since propane is in the oil and gas factor and propene is not assigned to a specific factor, HYPROPO2 is classified as a common RO_2. A total of 768 out of 1,130 peroxy radicals in the MCM have common precursors among the factors. To calculate the total production of NO_2 via RO_2 radical reaction with NO, and therefore gross O_3 production, we multiply the individual concentration of each RO_2 species in a given group by the concentration of NO and the rate constant for each time step. Lastly, we aggregate the results across all RO_2 species in the group and across all time steps in the simulation. The final product is the integrated contribution of a given set of representative VOCs to the total gross production of NO_2, and by extension O_3, for a given simulation.

Figure 5 displays the results of this RO_2 categorization and calculation of total NO_2 production for the baseline and high ONG simulations. The high oil and gas mixture produces more RO_2 radicals specific to oil and

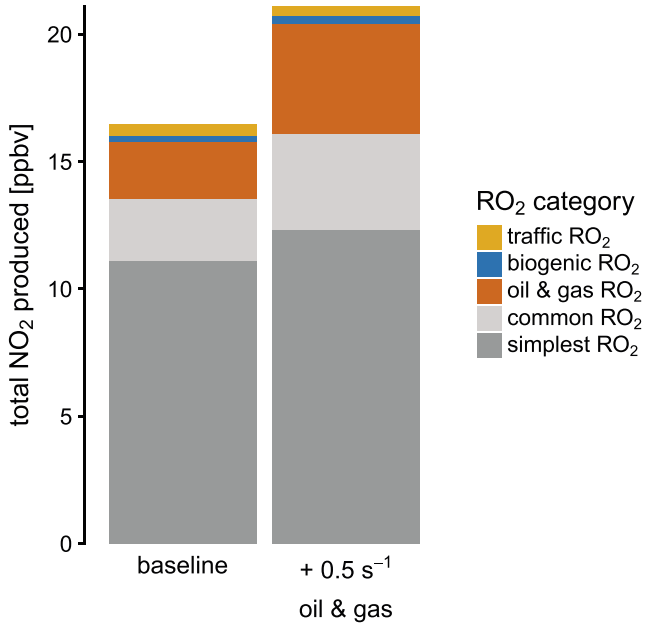

Figure 5. The sum of the RO_2 reactions that generate NO_2 for the baseline and high ONG 8-hr BOXMOX simulations, broken down by the precursor category of the RO_2 radical. Traffic, biogenic, and oil and gas RO_2 categories include RO_2 radicals that are solely products of parent species within each representative group of volatile organic compounds (VOCs). Common RO_2 radicals include those with precursors from multiple groups of precursor VOCs, and the simplest RO_2 radicals consist of the methyl-, ethyl-, and acetyl- peroxy radicals, which are common products of all the VOCs.

gas as compared to the baseline simulation. The high oil and gas mixture also produces more NO_2 in general than the baseline, and proportionately more simple and common RO_2 as well. Even though most of the individual trace gasses associated with the oil and gas activities (i.e., alkanes) have relatively low initial OHR, the abundances of these VOCs in the high ONG simulation are sufficient to create appreciable amounts of RO_2 radicals in a short period of time, in this case one photochemical day in the explicit MCM chemical framework. In this way, VOCs associated with the oil and gas activities appear to provide abundant opportunities to recycle NO_x through RO_2 production at multiple stages of oxidation, thus enhancing O_3 production. One possible pathway for this could be through the thermal decomposition of alkoxy radicals (RO) into an aldehyde and alkyl radical, which readily participate in further oxidation. For small ($\leq$3 carbon) RO, decomposition reactions are likely too slow as compared to reaction with O_2 to be relevant. For larger RO, however, thermal decomposition may be an important reaction pathway (Calvert et al., 2008; Orlando et al., 2003), especially on warmer days given the temperature dependence. Thermal decomposition of RO is included in the MCM, but the relative rates of these reactions are difficult to extract and examine. We considered trying to track RO radicals in the BOXMOX simulations similar to how we tracked RO_2. Naming conventions in the MCM make this difficult to do comprehensively as we have done for RO_2 species. Further research into the relative importance of this oxidation pathway in mixtures with high alkane abundances would be useful.

Lastly, we can use the BOXMOX simulations to investigate which measured VOCs are the most dominant PPN precursors. As discussed above, nearly any VOC can serve as a precursor to PAN, though the yields vary widely (Fischer et al., 2014; Roberts, 2008). In contrast, propanal is the main oxidation intermediate for PPN (Roberts et al., 2001, 2007). We test the sensitivity of PPN and PAN formation to a series of perturbations in individual precursors using the baseline simulation with a NO_x scaling factor of 1. We tested the sensitivity of PPN and PAN production to the full set of possible PPN precursors that were measured during the summer 2015 field campaign at BAO using a final set of simulations where the initial mixing ratio for each species was individually increased by 10% (Figures S1 and S2). All other precursors were set to the median mixing ratio observed during the campaign (the same as the baseline simulation). We find that propane and n-pentane are the dominant precursors for PPN in our simulations. Given that alkanes are attributed primarily to oil and gas activities in the NFRMA, these sensitivity results support the hypothesis that alkane emissions from oil and gas activities dominate the production of PPN and PAN in the NFRMA and are responsible for periods with high (>0.15) PPN/PAN ratios reported here and in Zaragoza et al. (2017).

5. Summary

Empirical observations and idealized box model simulations support the hypothesis that emissions from oil and gas extraction activities in the northern Colorado Front Range contribute to O_3 photochemical production in the region. We have four main conclusions.

1. The highest mixing ratios of PAN occur on the same days with the highest abundance of O_3, and these periods of elevated secondary species are consistently associated with ratios of PPN/PAN > 0.15. Additionally, when O_3 and the PPN/PAN ratio are most elevated, a large (25–45%) percent of the concurrently estimated VOC OHR is attributed to VOCs from oil and natural gas development. While a large percentage of VOC OHR from the oil and natural gas sector does not translate directly to O_3 production, the colocation of high PPN/PAN ratios suggest that emissions of VOCs from oil and natural gas production contribute to high O_3 days at BAO in summer 2015.
2. A larger percentage (30–60%) of the measured VOC OHR is attributed to isoprene when O_3 and PPN/PAN ratios are lower (<6 ppbv and <0.13). MPAN mixing ratios are also low, and MPAN/PAN

ratios are anticorrelated with O_3 abundance. This suggests that biogenic VOCs do not drive high O_3 events at BAO in summer 2015.

3. Based on the observations, the high ONG BOXMOX simulation is the most similar of our simulations to photochemistry on high O_3 days during our study period because (A) the abundances of VOCs used to initialize that simulation are within the bounds of what we observed on high O_3 days and (B) the PPN/PAN ratio increased from the baseline simulation to this high ONG simulation consistent with observations of higher PPN/PAN ratios on days with high O_3. It is clear in this simulation that even over a short period of time (i.e., one photochemical day) the oxidation of long-lived ONG VOCs with high abundances can still produce an appreciable amount of peroxy radicals. Thus, the idealized BOXMOX simulations support our empirical conclusion that VOCs from oil and natural gas activities contribute to O_3 production on high O_3 days. This is consistent with the findings from several other recent studies on O_3 in the northern Colorado Front Range using a variety of different methods (e.g., Cheadle et al., 2017; Evans & Helmig, 2017; McDuffie et al., 2016; Pfister, Flocke, et al., 2017).
4. Out of the VOC species that were measured, propane and several larger alkanes such as n-pentane are the dominant contributors to PPN production in the BOXMOX simulations. In the northern Colorado Front Range, these species predominately come from oil and natural gas sources (e.g., Abeleira et al., 2017; Gilman et al., 2013) and thus indicate that high ratios of PPN/PAN observed in the northern Colorado Front Range are driven by the oxidation of emissions from oil and natural gas production.

Acknowledgments
Funding for this work was provided by the US National Oceanic and Atmospheric Administration (NOAA) under award number NA14OAR4310148. Partial support for Jakob Lindaas was provided by the American Meteorological Society Graduate Fellowship. All data are available at the NOAA website (https://esrl.noaa.gov/csd/groups/csd7/measurements/2015songnex/ and aftp.cmdl.noaa.gov/data/ozwv/SurfaceOzone/BAO/). We appreciate all the logistical help at BAO provided by Dan Wolfe, Gerd Hübler, and Bruce Bartram (NOAA). We appreciate access to NOAA GMD ozone data provided by Audra McClure-Begley (NOAA). We thank Rebecca Hornbrook (NCAR) for providing the estimated photolysis rates used in the BOXMOX calculations.

References

Abeleira, A. J., & Farmer, D. K. (2017). Summer ozone in the northern Front Range metropolitan area: Weekend–weekday effects, temperature dependences, and the impact of drought. *Atmospheric Chemistry and Physics*, *17*(11), 6517–6529. https://doi.org/10.5194/acp-17-6517-2017

Abeleira, A. J., Pollack, I. B., Sive, B., Zhou, Y., Fischer, E. V., & Farmer, D. K. (2017). Source characterization of volatile organic compounds in the Colorado Northern Front Range metropolitan area during spring and summer 2015. *Journal of Geophysical Research: Atmospheres*, *122*, 3595–3613. https://doi.org/10.1002/2016JD026227

Bates, D. V. (2005). Ambient ozone and mortality. *Epidemiology*, *16*(4), 427–429. https://doi.org/10.1097/01.ede.0000165793.71278.ec

Brown, S. S., Thornton, J. A., Keene, W. C., Pszenny, A. A. P., Sive, B. C., DubÇ, W. P., et al. (2013). Nitrogen, aerosol composition, and halogens on a tall tower (NACHTT): Overview of a wintertime air chemistry field study in the front range urban corridor of Colorado. *Journal of Geophysical Research: Atmospheres*, *118*, 8067–8085. https://doi.org/10.1002/jgrd.50537

Calvert, J. G., Derwent, R. G., Orlando, J. J., Tyndall, G. S., & Wallington, T. J. (2008). *Mechanisms of atmospheric oxidation of the alkanes*. New York: Oxford University Press.

Camalier, L., Cox, W., & Dolwick, P. (2007). The effects of meteorology on ozone in urban areas and their use in assessing ozone trends. *Atmospheric Environment*, *41*(33), 7127–7137. https://doi.org/10.1016/j.atmosenv.2007.04.061

CDPHE. (2009). For recommended 8-hour ozone designations. Denver, CO:

Cheadle, L. C., Oltmans, S. J., Petron, G., Schnell, R. C., Mattson, E. J., Herndon, S. C., et al. (2017). Surface ozone in the Colorado Northern Front Range and the influence of oil and gas development during FRAPPE/DISCOVER-AQ in summer 2014. *Elementa: Science of the Anthropocene*, *5*. https://doi.org/10.1525/elementa.254

Ebben, C. J., Sparks, T. L., Wooldridge, P. J., Campos, T. L., Cantrell, C. A., Mauldin, R. L., et al. (2017). Evolution of NO_x in the Denver urban plume during the Front Range air pollution and photochemistry experiment. *Atmospheric Chemistry and Physics Discussions*, 1–13. https://doi.org/10.5194/acp-2017-671

Eilerman, S. J., Peischl, J., Neuman, J. A., Ryerson, T. B., Aikin, K. C., Holloway, M. W., et al. (2016). Characterization of ammonia, methane, and nitrous oxide emissions from concentrated animal feeding operations in northeastern Colorado. *Environmental Science & Technology*, *50*(20), 10,885–10,893. https://doi.org/10.1021/acs.est.6b02851

Emmerson, K. M., & Evans, M. J. (2009). Comparison of tropospheric gas-phase chemistry schemes for use within global models. *Atmospheric Chemistry and Physics*, *9*(5), 1831–1845. https://doi.org/10.5194/acp-9-1831-2009

EPA. (2015). Ground-level ozone—Regulatory actions. Retrieved from http://www3.epa.gov/ozonepollution/actions.html

Evans, J. M., & Helmig, D. (2017). Investigation of the influence of transport from oil and natural gas regions on elevated ozone levels in the northern Colorado Front Range. *Journal of the Air & Waste Management Association*, *67*(2), 196–211. https://doi.org/10.1080/10962247.2016.1226989

Farmer, D. K., Perring, A. E., Wooldridge, P. J., Blake, D. R., Baker, A., Meinardi, S., et al. (2011). Impact of organic nitrates on urban ozone production. *Atmospheric Chemistry and Physics*, *11*(9), 4085–4094. https://doi.org/10.5194/acp-11-4085-2011

Fischer, E. V., Jacob, D. J., Yantosca, R. M., Sulprizio, M. P., Millet, D. B., Mao, J., et al. (2014). Atmospheric peroxyacetyl nitrate (PAN): A global budget and source attribution. *Atmospheric Chemistry and Physics*, *14*(5), 2679–2698. https://doi.org/10.5194/acp-14-2679-2014

Fowler, D. (1992). *Effects of acidic pollutants on terrestrial ecosystems*. Amsterdam: Elsevier.

Gilman, J. B., Lerner, B. M., Kuster, W. C., & de Gouw, J. A. (2013). Source signature of volatile organic compounds from oil and natural gas operations in northeastern Colorado. *Environmental Science & Technology*, *47*(3), 1297–1305. https://doi.org/10.1021/es304119a

Guenther, A., Karl, T., Harley, P., Wiedinmyer, C., Palmer, P. I., & Geron, C. (2006). Estimates of global terrestrial isoprene emissions using MEGAN (model of emissions of gases and aerosols from nature). *Atmospheric Chemistry and Physics*, *6*(11), 3181–3210. https://doi.org/10.5194/acp-6-3181-2006

Haagen-Smit, A. J., & Fox, M. M. (1956). Ozone formation in photochemical oxidation of organic substances. *Industrial and Engineering Chemistry*, *48*(9), 1484–1487. https://doi.org/10.1021/ie51400a033

Halliday, H. S., Thompson, A. M., Wisthaler, A., Blake, D. R., Hornbrook, R. S., Mikoviny, T., et al. (2016). Atmospheric benzene observations from oil and gas production in the Denver-Julesburg Basin in July and August 2014. *Journal of Geophysical Research: Atmospheres*, *121*, 11,055–11,074. https://doi.org/10.1002/2016JD025327

Ito, K., De Leon, S. F., & Lippmann, M. (2005). Associations between ozone and daily mortality—Analysis and meta-analysis. *Epidemiology*, *16*(4), 446–457. https://doi.org/10.1097/01.ede.0000165821.90114.7f

Jacob, D. J., Logan, J. A., Yevich, R. M., Gardner, G. M., Spivakovsky, C. M., Wofsy, S. C., et al. (1993). Simulation of summertime ozone over North America. *Journal of Geophysical Research*, *98*, 14,797–14,816. https://doi.org/10.1029/93JD01223

Jenkin, M. E., Young, J. C., & Rickard, A. R. (2015). The MCM v3.3.1 degradation scheme for isoprene. *Atmospheric Chemistry and Physics*, *15*(20), 11,433–11,459. https://doi.org/10.5194/acp-15-11433-2015

Jin, L., Tonse, S., Cohan, D. S., Mao, X., Harley, R. A., & Brown, N. J. (2008). Sensitivity analysis of ozone formation and transport for a Central California air pollution episode. *Environmental Science & Technology*, *42*(10), 3683–3689. https://doi.org/10.1021/es072069d

Kelly, T. J., Stedman, D. H., & Kok, G. L. (1979). Measurements of H2O2 and HNO3in rural air. *Geophysical Research Letters*, *6*, 375–378. https://doi.org/10.1029/GL006i005p00375

Knote, C., Tuccella, P., Curci, G., Emmons, L., Orlando, J. J., Madronich, S., et al. (2015). Influence of the choice of gas-phase mechanism on predictions of key gaseous pollutants during the AQMEII phase-2 intercomparison. *Atmospheric Environment*, *115*(Supplement C), 553–568. https://doi.org/10.1016/j.atmosenv.2014.11.066

Lindaas, J., Farmer, D. K., Pollack, I. B., Abeleira, A., Flocke, F., Roscioli, R., et al. (2017). Changes in ozone and precursors during two aged wildfire smoke events in the Colorado Front Range in summer 2015. *Atmospheric Chemistry and Physics*, *17*(17), 10,691–10,707. https://doi.org/10.5194/acp-17-10691-2017

Madronich, S. (1992). Implications of recent total atmospheric ozone measurements for biologically active ultraviolet radiation reaching the Earth's surface. *Geophysical Research Letters*, *19*, 37–40. https://doi.org/10.1029/91GL02954

McClure-Begley, A., Petropavlovskikh, I., & Oltmans, S. (2014). NOAA Global Monitoring Surface Ozone Network. BAO, June 2015–September 2015. National Oceanic and Atmospheric Administration, Earth Systems Research Laboratory Global Monitoring Division. Boulder, CO. https://doi.org/10.7289/V5P8WBF

McDuffie, E. E., Edwards, P. M., Gilman, J. B., Lerner, B. M., Dubé, W. P., Trainer, M., et al. (2016). Influence of oil and gas emissions on summertime ozone in the Colorado Northern Front Range. *Journal of Geophysical Research: Atmospheres*, *121*, 8712–8729. https://doi.org/10.1002/2016JD025265

Millet, D. B., Guenther, A., Siegel, D. A., Nelson, N. B., Singh, H. B., de Gouw, J. A., et al. (2010). Global atmospheric budget of acetaldehyde: 3-D model analysis and constraints from in-situ and satellite observations. *Atmospheric Chemistry and Physics*, *10*(7), 3405–3425. https://doi.org/10.5194/acp-10-3405-2010

Monks, P. S., Archibald, A. T., Colette, A., Cooper, O., Coyle, M., Derwent, R., et al. (2015). Tropospheric ozone and its precursors from the urban to the global scale from air quality to short-lived climate forcer. *Atmospheric Chemistry and Physics*, *15*(15), 8889–8973. https://doi.org/10.5194/acp-15-8889-2015

Orlando, J. J., Tyndall, G. S., & Wallington, T. J. (2003). The atmospheric chemistry of alkoxy radicals. *Chemical Reviews*, *103*(12), 4657–4690. https://doi.org/10.1021/cr020527p

Pétron, G., Frost, G., Miller, B. R., Hirsch, A. I., Montzka, S. A., Karion, A., et al. (2012). Hydrocarbon emissions characterization in the Colorado Front Range: A pilot study. *Journal of Geophysical Research*, *117*, D04304. https://doi.org/10.1029/2011JD016360

Pétron, G., Karion, A., Sweeney, C., Miller, B. R., Montzka, S. A., Frost, G. J., et al. (2014). A new look at methane and nonmethane hydrocarbon emissions from oil and natural gas operations in the Colorado Denver-Julesburg Basin. *Journal of Geophysical Research: Atmospheres*, *119*, 6836–6852. https://doi.org/10.1002/2013JD021272

Pfister, G. G., Flocke, F., Hornbrook, R. S., Orlando, J. J., Lee, S., & Schroeder, J. R. (2017). Process-based and regional source impact analysis for FRAPPÉ and DISCOVER-AQ 2014. Boulder, CO. Retrieved from https://www.colorado.gov/airquality/tech_doc_repository.aspx?action=open&file=FRAPPE-NCAR_Final_Report_July2017.pdf

Pfister, G. G., Reddy, P. J., Barth, M. C., Flocke, F. F., Fried, A., Herndon, S. C., et al. (2017). Using observations and source-specific model tracers to characterize pollutant transport during FRAPPÉ and DISCOVER-AQ. *Journal of Geophysical Research: Atmospheres*, *122*, 10,510–10,538. https://doi.org/10.1002/2017JD027257

Reddy, P. J., & Pfister, G. G. (2016). Meteorological factors contributing to the interannual variability of midsummer surface ozone in Colorado, Utah, and other western U.S. states. *Journal of Geophysical Research: Atmospheres*, *121*, 2434–2456. https://doi.org/10.1002/2015JD023840

Rhew, R. C., Deventer, M. J., Turnipseed, A. A., Warneke, C., Ortega, J., Shen, S., et al. (2017). Ethene, propene, butene and isoprene emissions from a ponderosa pine forest measured by relaxed eddy accumulation. *Atmospheric Chemistry and Physics*, *17*(21), 13,417–13,438. https://doi.org/10.5194/acp-17-13417-2017

Roberts, J. M. (2008). PAN and Related Compounds. In R. Koppmann (Ed.), *Volatile organic compounds in the atmosphere* (pp. 221–268). Oxford, UK: Blackwell Publishing Ltd.

Roberts, J. M., Jobson, B. T., Kuster, W., Goldan, P., Murphy, P., Williams, E., et al. (2003). An examination of the chemistry of peroxycarboxylic nitric anhydrides and related volatile organic compounds during Texas Air Quality Study 2000 using ground-based measurements. *Journal of Geophysical Research*, *108*(D16), 4495. https://doi.org/10.1029/2003JD003383

Roberts, J. M., Marchewka, M., Bertman, S. B., Sommariva, R., Warneke, C., de Gouw, J., et al. (2007). Measurements of PANs during the New England Air Quality Study 2002. *Journal of Geophysical Research*, *112*, D20306. https://doi.org/10.1029/2007JD008667

Roberts, J. M., Stroud, C. A., Jobson, B. T., Trainer, M., Hereid, D., Williams, E., et al. (2001). Application of a sequential reaction model to PANs and aldehyde measurements in two urban areas. *Geophysical Research Letters*, *28*, 4583–4586. https://doi.org/10.1029/2001GL013507

Roberts, J. M., Williams, J., Baumann, K., Buhr, M. P., Goldan, P. D., Holloway, J., et al. (1998). Measurements of PAN, PPN, and MPAN made during the 1994 and 1995 Nashville intensives of the southern oxidant study: Implications for regional ozone production from biogenic hydrocarbons. *Journal of Geophysical Research*, *103*, 22,473–22,490. https://doi.org/10.1029/98JD01637

Sandu, A., Daescu, D. N., & Carmichael, G. R. (2003). Direct and adjoint sensitivity analysis of chemical kinetic systems with KPP: Part I—Theory and software tools. *Atmospheric Environment*, *37*(36), 5083–5096. https://doi.org/10.1016/j.atmosenv.2003.08.019

Sillman, S. (1999). The relation between ozone, NO_x, and hydrocarbons in urban and polluted rural environments. *Atmospheric Environment*, *33*(12), 1821–1845. https://doi.org/10.1016/S1352-2310(98)00345-8

Sillman, S., Al-Wali, K. I., Marsik, F. J., Nowacki, P., Samson, P. J., Rodgers, M. O., et al. (1995). Photochemistry of ozone formation in Atlanta, GA-models and measurements. *Atmospheric Environment*, *29*(21), 3055–3066. https://doi.org/10.1016/1352-2310(95)00217-M

Sillman, S., & Samson, P. J. (1995). Impact of temperature on oxidant photochemistry in urban, polluted rural and remote environments. *Journal of Geophysical Research*, *100*, 11,497–11,508. https://doi.org/10.1029/94JD02146

Sommariva, R., de Gouw, J. A., Trainer, M., Atlas, E., Goldan, P. D., Kuster, W. C., et al. (2011). Emissions and photochemistry of oxygenated VOCs in urban plumes in the Northeastern United States. *Atmospheric Chemistry and Physics*, *11*(14), 7081–7096. https://doi.org/10.5194/acp-11-7081-2011

Sullivan, J. T., McGee, T. J., Langford, A. O., Alvarez, R. J., Senff, C. J., Reddy, P. J., et al. (2016). Quantifying the contribution of thermally driven recirculation to a high-ozone event along the Colorado Front Range using lidar. *Journal of Geophysical Research: Atmospheres*, *121*, 10,377–10,390. https://doi.org/10.1002/2016JD025229

Swarthout, R. F., Russo, R. S., Zhou, Y., Hart, A. H., & Sive, B. C. (2013). Volatile organic compound distributions during the NACHTT campaign at the Boulder Atmospheric Observatory: Influence of urban and natural gas sources. *Journal of Geophysical Research: Atmospheres*, *118*, 610,614–610,637. https://doi.org/10.1002/jgrd.50722

Tevlin, A. G., Li, Y., Collett, J. L., McDuffie, E. E., Fischer, E. V., & Murphy, J. G. (2017). Tall tower vertical profiles and diurnal trends of ammonia in the Colorado Front Range. *Journal of Geophysical Research: Atmospheres*, *122*, 12,468–12,487. https://doi.org/10.1002/2017JD026534

Thompson, C. R., Hueber, J., & Helmig, D. (2014). Influence of oil and gas emissions on ambient atmospheric non-methane hydrocarbons in residential areas of northeastern Colorado. *Elementa: Science of the Anthropocene*, *2*, 000035. https://doi.org/10.12952/journal.elementa.000035

Thornton, J. A., Wooldridge, P. J., Cohen, R. C., Martinez, M., Harder, H., Brune, W. H., et al. (2002). Ozone production rates as a function of NOx abundances and HO_x production rates in the Nashville urban plume. *Journal of Geophysical Research*, *107*(D12), 4146. https://doi.org/10.1029/2001JD000932

Townsend-Small, A., Botner, E. C., Jimenez, K. L., Schroeder, J. R., Blake, N. J., Meinardi, S., et al. (2016). Using stable isotopes of hydrogen to quantify biogenic and thermogenic atmospheric methane sources: A case study from the Colorado Front Range. *Geophysical Research Letters*, *43*, 11,462–411,471. https://doi.org/10.1002/2016GL071438

Vu, K. T., Dingle, J. H., Bahreini, R., Reddy, P. J., Apel, E. C., Campos, T. L., et al. (2016). Impacts of the Denver cyclone on regional air quality and aerosol formation in the Colorado front range during FRAPPÉ 2014. *Atmospheric Chemistry and Physics*, *16*(18), 12,039–12,058. https://doi.org/10.5194/acp-16-12039-2016

Wang, L., Newchurch, M. J., Alvarez Ii, R. J., Berkoff, T. A., Brown, S. S., Carrion, W., et al. (2017). Quantifying TOLNet ozone lidar accuracy during the 2014 DISCOVER-AQ and FRAPPÉ campaigns. *Atmospheric Measurement Techniques*, *10*(10), 3865–3876. https://doi.org/10.5194/amt-10-3865-2017

Wild, R. J., Dubé, W. P., Aikin, K. C., Eilerman, S. J., Neuman, J. A., Peischl, J., et al. (2017). On-road measurements of vehicle NO2/NOx emission ratios in Denver, Colorado, USA. *Atmospheric Environment*, *148*, 182–189. https://doi.org/10.1016/j.atmosenv.2016.10.039

Williams, J., Roberts, J. M., Fehsenfeld, F. C., Bertman, S. B., Buhr, M. P., Goldan, P. D., et al. (1997). Regional ozone from biogenic hydrocarbons deduced from airborne measurements of PAN, PPN, and MPAN. *Geophysical Research Letters*, *24*, 1099–1102. https://doi.org/10.1029/97GL00548

Young, W. A., Shaw, D. B., & Bates, D. V. (1964). Effect of low concentrations of ozone on pulmonary function in man. *Journal of Applied Physiology*, *19*(4), 765–768. https://doi.org/10.1152/jappl.1964.19.4.765

Zaragoza, J., Callahan, S., McDuffie, E. E., Kirkland, J., Brophy, P., Durrett, L., et al. (2017). Observations of acyl peroxy nitrates during the Front Range Air Pollution and Photochemistry Éxperiment (FRAPPÉ). *Journal of Geophysical Research: Atmospheres*, *122*, 12,416–12,432. https://doi.org/10.1002/2017JD027337